Mechanical Fluctuations of the Membrane–Skeleton Are Dependent on F-Actin ATPase in Human Erythrocytes

Shmuel Tuvia, Shlomo Levin, Arkady Bitler, and Rafi Korenstein

Department of Physiology and Pharmacology, Sackler Faculty of Medicine, Tel-Aviv University, 69978 Tel-Aviv, Israel

Abstract. Cell membrane fluctuations (CMF) of human erythrocytes, measured by point dark field microscopy, were shown to depend, to a large extent, on intracellular MgATP (Levin, S.V., and R. Korenstein. 1991. *Biophys. J.* 60:733–737). The present study extends that investigation and associates CMF with F-actin's ATPase activity. MgATP was found to reconstitute CMF in red blood cell (RBC) ghosts and RBC skeletons to their levels in intact RBCs, with an apparent K_d of 0.29 mM. However, neither non-hydrolyzable ATP analogues (AMP-PNP, ATPγS) nor hydrolyzable ones (ITP, GTP), were able to elevate CMF levels. The inhibition of ATPase activity associated with the RBC's skeleton, carried out either by the omission of the MgATP substrate or by the use of several inhibitors (vanadate, phalloidin, and DNase I), resulted in a strong decrease of CMF. We suggest that the actin's ATPase, located at the pointed end of the short actin filament, is responsible for the MgATP stimulation of CMF in RBCs.

Movements of the cell surface are a common characteristic property of animal cells. Recently, a non-locomotive process, consisting of reversible submicron fluctuations of the cell membrane surface in the frequency range of 0.3–30 Hz has been described to be possessed by various cells. These cell membrane fluctuations (CMF)[1] have been observed in different cell types including red blood cells (RBCs) (Krol et al., 1990, Levin and Korenstein, 1991, Peterson et al., 1991., Tuvia et al., 1992*a*, Strey et al., 1995) monocytes, lymphocytes, 3T6 fibroblasts, cardiomyocytes (Krol et al., 1990), and murine lymphoma B and T cells (Mittelman et al., 1991, 1994). CMF consist of local (~0.25 μm^2) out-of-plane cell surface displacements (20–300 nm), which reflect the local bending deformability of the cell surface. CMF were shown to be directly correlated with the efficiency of filterability of white and red blood cells through pores smaller than their dimensions (Tuvia et al., 1992*b*; Zamir et al., 1992; Mittelman et al., 1994). A higher level of CMF and cell filterability was found in T lymphoma cells possessing a high metastatic potential than in their non-metastatic subclones (Mittelman et al., 1994). CMF in RBCs have, so far, been viewed as thermal fluctuations of the membrane–skeleton complex (Strey et al., 1995). In an attempt to examine whether surface fluctuations are dependent on metabolic energy, we have previously shown that CMF of RBCs depend, to a large extent, on intracellular MgATP (Levin and Korenstein, 1991). The effect of MgATP on CMF was examined in several types of RBC ghosts showing that CMF can be reconstituted to the same levels as in intact RBCs, in the presence of MgATP. Moreover, the recent observation that CMF energy is attenuated by the medium's macroviscosity, suggests that CMF are driven by a metabolic, in addition to a thermal source (Tuvia et al., 1997). The present study extends our previous examination of the effect of intracellular MgATP on CMF and associates CMF with F-actin's ATPase activity.

Materials and Methods

Preparation of RBCs, Saponin Ghosts, and Triton X-100 Shells for Measurement of Cell Membrane Fluctuations

Fresh human RBCs were obtained immediately before each experiment from a healthy donor. 50–100 μl of blood were diluted 50-fold in a PBS solution containing: 130 mM NaCl, 20 mM K/Na phosphate buffer, 10 mM glucose, 1 mg/ml BSA, pH 7.4. The addition of 1 mg/ml BSA to the PBS solutions was essential for preserving the biconcave shape of RBCs. RBCs were washed twice with PBS by centrifugation (1,500 rpm, 2 min at 20°C), the puffy coat was removed, and then the amount of RBCs, in the final suspension, was adjusted to ~5×10^6 cells/ml. For long-term studies, penicillin/streptomycin (0.5 unit/ml) was added to the PBS solution. A RBC suspension in PBS was introduced into the experimental chamber at a low amount, so that the volume ratio of cells/solution in the chamber was 1:3,000. The experimental chamber consisted of two coverglasses separated by a distance of 0.2 mm. Incubation in chamber for 20 min, at 22–24°C, allowed the RBCs to firmly adhere to the glass substratum. In some experiments we covered the glass with low concentration (5–20 μg/ml) of poly-L-lysine (mol wt = 65.5 kD) and made sure, using phase contrast mi-

Address all correspondence to Dr. R. Korenstein, Department of Physiology and Pharmacology, Sackler Faculty of Medicine, Tel-Aviv University, 69978 Tel-Aviv, Israel. Tel.: 972-3-6406042. Fax: 972-3-6409113. E-mail: korens@post.tau.ac.il

1. *Abbreviations used in this paper*: CMF, cell membrane fluctuations; RBC, red blood cell.

croscopic observation, that the cells' shape did not change from their biconcave shape.

Preparation of non-resealed RBC ghosts was carried out using a procedure similar to the one described for the preparation of RBCs up to the step where RBCs were attached to the coverglass. Hemolysis of the RBCs was performed by perfusing the chamber with 50 μl of 0.0075% saponin in PBS for 30 s, and then washing out the saponin by adding 150 μl of "KCl solution" (130 mM KCl, 20 mM K/Na phosphate buffer, 10 mM glucose, 0.2 mM PMSF, 1 mg/ml BSA, pH 7.8). To determine the size of the holes produced in the membrane of RBC ghosts, after exposure to saponin, intact RBCs were loaded, at first, with 486-kD Dextran-FITC. The incorporation of this fluorescent molecular probe was carried out by subjecting intact RBC suspension to a train of low voltage pulses by a procedure described previously (Rosemberg and Korenstein, 1997). After loading, which was revealed by fluorescence microscopy, the RBCs were treated with 0.0075% saponin in PBS, followed by a wash with KCl solution. This resulted in the loss of fluorescence demonstrating that the RBC ghosts are leaky for molecules of ≤500 kD.

RBC Triton X-100 shells (skeletons) were prepared by perfusing RBCs attached to a coverglass (0.1% hematocrit) by PBS containing 0.0075% saponin. The produced RBC ghosts were further perfused with 0.04% of Triton X-100 in a KCl solution (400 mg Triton X-100 per 1 ml of packed RBC ghosts). Finally the skeletons were washed further with additional volumes of KCl solution. The skeletons maintained a similar size and shape (see Fig. 7) to that of RBC saponin ghosts for ~20–30 min, before major shrinkage of the skeleton took place. This irreversible shrinkage of the skeleton could be detected either by dark field microscopy or by the time-independent increase in light scattering from the skeleton.

Measurements of Membrane Fluctuations by Point Dark Field Microscopy

The measurement of local mechanical fluctuations of the cell membrane is carried out on RBC, RBC ghosts and RBC skeletons using an optical method based on Point Dark Field Microscopy (Krol et al., 1990; Levin and Korenstein, 1991). We illuminate a small area (0.25–1 μm^2) at the edge of cells attached to a cover glass and record cell membrane displacements by monitoring the time-dependent changes of light reflection and scattering, using the experimental set-up shown in Fig. 1 *A*. The fluctuation of the light intensity depends on the changes in the membrane area moving in and out of the focused light spot near the cell's edge (Fig. 1 *B*). The time-dependent changes of the scattered light intensity (ΔI) are normalized via division by the time-independent scattered light (I). The analysis of the time series of scattered light intensity is carried out in terms of normalized maximal amplitude of the scattered light intensity ($\Delta I_{max}/I$)%. The sensitivity of the experimental set-up was ~1%. All measurements are carried out at 25°–28°C. The measurements of fluctuation amplitudes are taken over a long time period, ≤90 min, under steady-state conditions (constant maximum levels of fluctuation). The variation coefficient (SD/mean) of maximal CMF amplitudes measured in control RBC populations of 20–40 cells from a single donor was ~10%, whereas the variation coefficient of CMF measured in RBCs from 10 donors was elevated to 15–20%.

Fast Fourier Transformation of fluctuation traces, of ≤10 repeated measurements, was carried out for light scattering measurements at the cell's edge. Power spectra of repetitive measurements was averaged both over time and frequency range. The calculation of the standard deviation of the squared amplitude of the time-dependent fluctuation at each frequency enables us to evaluate the stationary characteristic of the power spectra. Control experiments carried out after exposure of RBCs to PBS solution containing 0.01% glutaraldehyde, a cross-linking agent, resulted in complete abolishment of CMF.

An additional, quantitative, examination of CMF recordings was performed using amplitude distribution analysis. The scattering from each surface area was recorded for 55 or 110 s (sampling rate of 75 points/s). These tracings were analyzed by grouping the amplitudes according to their sizes and counting the normalized frequency of appearance of each amplitude value in the recording (the relative number of events belonging to a chosen amplitude group divided by the total number of events in the recording). Further, a plot of the relative number of events versus corresponding values of fluctuations yields the amplitude histograms, which are presented in Figs. 3 and 9. All curves are bell shaped, enabling us to avoid certain problems arising when trying to estimate the power spectrum bandwidth that demands precise definition of the maximum point on the left side of the power spectrum. As the power spectrum strongly drops, the error increases. An additional complication arises in the analysis of the low frequency region of the power spectrum, which is prone to high distortion by the high-pass filter. No such problem exists when the bell-shaped distribution curves are analyzed, as the commonly used characteristic of the amplitude distribution is the half-width of the distribution curve, which is related to the fluctuation energy. Thus, the half-width increases when the fluctuation energy increases.

ATP Depletion

Reversible ATP depletion in RBCs was obtained by prolonged incubation in glucose-free PBS for 24 h at 37°C and for 16 h at 4°C. Irreversible ATP depletion in RBCs was carried out by using several procedures: (*a*) incubation without glucose, in the presence of 6 mM iodoacetamide (a powerful inhibitor of glyceraldehyde-3-phosphate dehydrogenase) for 5 h at 37°C; (*b*) incubation without glucose, in the presence of 10 mM inosine and 6 mM iodoacetamide, for 1 h at 37°C; (*c*) incubation without glucose, in the presence of 10 mM inosine and 6 mM iodoacetamide, for 5 h at 37°C.

The addition of glycolytic substrates, in the presence of iodoacetamide, speeds up ATP depletion because the substrate consumes ATP, whereas glycolytic ATP production is blocked (Lew and Ferreira, 1978). To achieve an even faster ATP depletion, glucose was replaced by the more

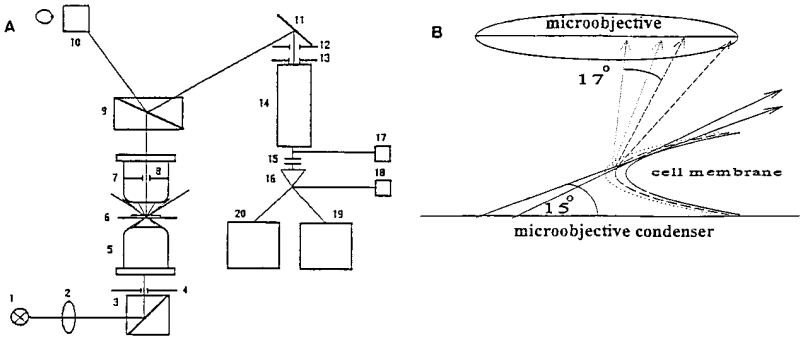

Figure 1. Schematic diagram of the electro-optic set-up for measuring cell membrane fluctuations by Point Dark Field Microscopy (*A*). A polychromatic light from a halogen lamp (or a high pressure mercury lamp) (*1*) passed through a collector lens (*2*), deflected at a right angle by a rectangular prism (*3*), and passed through a variable rectangular slit (*4*) (50 × 50 μm up to 100 × 100 μm). The light emerging from the slit passed through a catadioptric microobjective (*5*)(×100, NA 1.3), which focuses the light on an area of 0.25–1 μm^2, at the cell's edge of a RBC attached to a cover-glass (*6*), forming an annular light cone of 15°–20° relative to the plane of the coverglass surface of the experimental chamber (*B*). The scattered light is collected (at an annular angle of 3°–17° relative to the optic axis of the microobjective, perpendicular to the cover glass), by a water immersion microobjective (×30, NA 0.9) (*7*) equipped with an iris diaphragm (*8*). After passing through a beamsplitter (*9*), one beam of the scattered light passed through an ocular (*10*), while the other beam was deflected by a mirror (*11*) through a pinhole slit (*12*, *13*), and then detected by a photomultiplier (*14*). The time-dependent photocurrent of the photomultiplier, passed via a condenser (*15*), amplified by a Grass 79C amplifier (*16*) (with high and low pass filters of 0.3 Hz and 35 Hz, respectively), interfaced to a PC via an A/D converter (*20*). Since the submicron cell membrane fluctuations occur in the frequency range of 0.3–30 Hz, we used a sampling rate of 75 Hz. The time-independent light intensity of the scattered light was measured by a voltmeter (*17*), whereas the time-dependent component was observed by an oscilloscope (*18*), and measured by a recorder (*19*) or PC (*20*).

efficient inosine. Thus, incubation of RBCs in the presence of 10 mM inosine and 6 mM iodoacetamide reduces the intracellular ATP to a level of 1–5 μM in <1 h of incubation at 37°C (Lew and Gracia-Sancho, 1989). The low ATP level in inosine-iodoacetamide–treated cells is maintained by rapid turnover for many hours (at ~200 μM/h), probably sustained by the large reserves of 2,3 diphosphoglycerate within the cells (Glynn and Lew, 1970). ATP levels in ATP-depleted RBCs were restored by overnight preincubation at 4°C in a medium containing 10 mM glucose.

Shape changes of RBC accompany both reversible and irreversible ATP depletion experiments, leading to a heterologous population of RBCs including echinocytes and stomatocytes in addition to discocytes. Thus, ATP depletion under reversible conditions (24 h at 37°C in glucose-free medium) leads to a 10–20% decrease in the discocyte population. When ATP depletion was carried out under irreversible conditions it seemed that most RBCs prepared as described by procedure *b*, kept their biconcave discocyte shape, whereas RBCs that were prepared as described in *a* led to a significant number of stomatocytes. When incubation was carried out under the conditions described for procedure *c* the main population of cells consisted of echinocytes. To test the effect of ATP depletion on the fluctuation amplitudes, without the necessity of considering the possible effect of shape change, we measured CMF in RBCs possessing normal discoid shape only.

Heat Treatment of RBCs

Human erythrocytes were attached to the cover glass of the experimental chamber. Heat treatment was carried out by incubating RBCs in the chamber at 50°C for 5 min.

Analysis of the Effect of Vanadate on Membrane–Skeleton Phosphorylation by Immunoblotting

RBCs were suspended in PBS containing 10 mM glucose, 0.8 mM Mg^{+2}, 1 mM Ca^{+2}, and 30 μM vanadate (buffer A) at 4% hematocrit, and incubated for 15 min in PBS at 37°C. Next, RBC ghosts were prepared by hemolyzing the cells in 5 mM sodium phosphate buffer, pH 8, containing 1 mM EDTA, 0.1 mM PMSF, in the presence and absence of 30 mM vanadate. The ghosts were washed with the same buffer, then further washed with 5 mM NaCl, and 0.1 mM PMSF, in the presence of 30 μM vanadate to obtain hemoglobin-free ghosts. For the identification of the phosphorylated membrane–skeleton proteins, aliqouts were solubilized, and boiled for 2 min in Laemmli's SDS sample buffer.

Proteins of the solubilized RBC ghosts were resolved by 7.5% SDS/PAGE, followed by transfer to nitrocellulose membranes and immunoblotting analysis as previously described (Zipser and Kosower, 1996). For the analysis of phosphotyrosine, the nitrocellulose membranes were blocked in TTBS solution (20 mM Tris, pH 7.4, 150 mM NaCl, 0.1% Tween-20, containing 3% BSA and 0.05% NaN_3), and then incubated for 1 h with an anti-phosphotyrosine mAb (BioMakor, Rehovot, Israel) diluted 1:2,000. After washing with TTBS containing 2% lowfat dried milk and 0.2% BSA, the membranes were incubated for 45 min with sheep anti–mouse peroxidase-conjugated antibodies (Amersham Corp., Arlington Heights, IL), washed in TTBS, and then analyzed using the ECL detection system (Amersham Corp.). A similar procedure was carried out for the analysis of phosphoserine proteins by using polyclonal anti-phosphoserine (Zymed Laboratories, Inc., South San Francisco, CA). The antibody was diluted 1:1,000 and goat anti–rabbit peroxidase-conjugated antibodies were used as secondary antibodies.

Direct phosphorylation of RBC ghosts (100 μg) was carried out in Tris-KCl buffer (5 mM Tris, pH 7.4, 5 mM KCl) containing 1 mM MgATP in the presence or absence of 10 μM vanadate. After preincubation for 10 min at 4°C, 150 mM KCl solution was added and the ghosts were incubated for 15 more min at 37°C. The phosphorylation was terminated upon addition of Laemmli's SDS sample buffer and analyzed by immunoblotting.

Exposure of RBC Ghosts to Phalloidin, DNase I and Cytochalasins (B and D)

The effects of phalloidin, in the concentration range of 0.44–50 μM, or 0.16 μM deoxyribonuclease I (DNase I) on CMF were studied in RBC ghosts. The CMF level of RBC ghosts was elevated upon perfusion with KCl solution containing 1 mM MgATP. After this elevation the RBC ghosts were perfused and incubated for 20 min at room temperature, in the presence of KCl solution containing 1 mM MgATP and the appropriate amounts of phalloidin or DNase I. An alternative approach for studying the effects of phalloidin or DNase I was to preincubate RBC ghosts with KCl solution containing either phalloidin or DNase I, followed by a perfusion of a KCl solution to which 1 mM MgATP was added. The effect of dihydrocytochalasin B and cytochalasin D on CMF was examined by incubating RBCs with these agents. RBCs were exposed to 2 μM and 4 μM dihydrocytochalasin B in PBS for 24 h at room temperature and for 30 min at 37°C, respectively. RBCs were exposed to 20 μM cytochalasin D for 2 h at room temperature.

To examine the spatial distribution of actin in RBC ghosts we used fluorescently labeled phalloidin-rhodamine and DNase I–FITC. The labeling was carried out on RBC ghosts adhered to the cover-glass, prepared by the procedure described above. The RBC ghosts were preincubated for 10 min with KCl solution containing 1 mM MgATP. After this incubation period, they were washed and incubated for 20 min at 4°C with KCl solution containing 1 mM MgATP, in the presence of 0.5% glutaraldehyde or in its absence. The RBC ghosts were washed twice with a KCl solution, and then incubated with 4.4 μM phalloidin-rhodamine (Molecular Probes, Inc., Eugene, OR) alone or with a combination of 4.4 μM phalloidin-rhodamine and 35 nM DNase I–FITC (Molecular Probes, Inc.). The incubation with the fluorescent probes was carried out for 20 min followed by an extensive fivefold slow wash of the RBC ghosts with a KCl solution.

The spatial distribution of the fluorescent probes was analyzed via a three-dimensional optical sectioning using a confocal inverted laser scanning microscope (LSM 410; Carl Zeiss Inc., Thornwood, NY). The three-dimensional analysis shows that non-resealed RBC ghosts possessed dimensions similar to those of intact adhered RBCs, but have a flat rather than a biconcave shape.

Results

Effect of ATP Depletion from RBCs on Cell Membrane Fluctuations

Reversible and irreversible depletion of ATP were carried

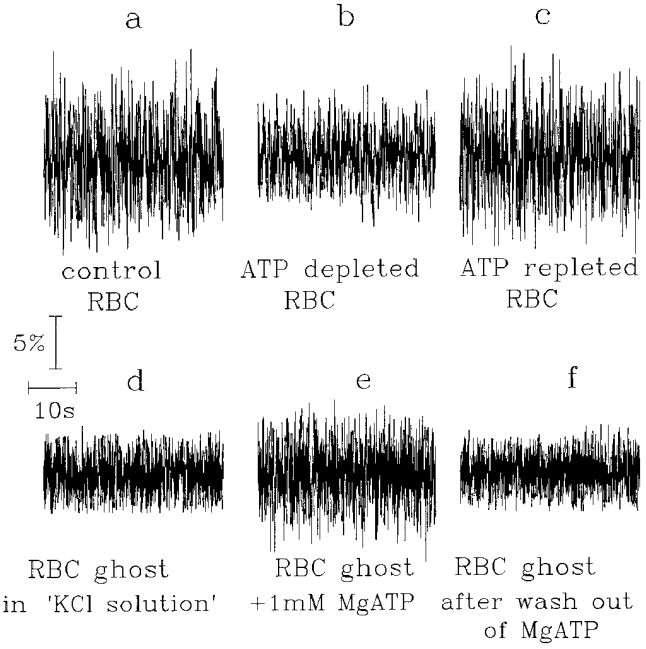

Figure 2. Recordings of time-dependent light scattering from the side surface of human RBCs and RBC ghosts in the presence and absence of intracellular ATP. (*a*) CMF of a normal human RBC; (*b*) CMF of an ATP-depleted RBC (where depletion was carried out by incubating RBCs in glucose-free PBS solution for 16 h at 4°C); (*c*) CMF of a RBC after repletion of the intracellular ATP level; (*d*) CMF of a RBC ghost perfused with a KCl solution; (*e*) CMF of a RBC ghost perfused with KCl solution in the presence of 1 mM MgATP; (*f*) CMF of a RBC ghost perfused with KCl solution devoid of MgATP.

out by depriving RBCs from a glycolysis substrate or by exposure to glycolytic inhibition. Reversible ATP depletion was obtained by prolonged incubation of RBCs for 24 h at 37°C in a glucose-free PBS. This resulted in an ~40% decrease of the maximal fluctuation amplitude (Fig. 2; Table I). However, when carrying out the same depletion procedure for 16 h at 4°C, the CMF amplitude declined by only 30%. In both cases, the examination of the storage effect per se on CMF level has shown that the CMF amplitude of 16.5 ± 3% (n = 122, three donors) (mean ± SD where n is the number of measured RBCs) in freshly prepared RBCs was only marginally attenuated upon the long preincubation in the presence of glucose at either 37° or 4°C.

To examine whether the effect of ATP depletion on CMF is reversible, ATP levels in ATP-depleted RBCs were restored, by overnight preincubation at 4°C in a medium containing 10 mM glucose. After the repletion of intracellular ATP, the level of CMF was restored, resulting in a level comparable to that in control RBCs. Irreversible depletion of intracellular ATP, by the three different procedures, was accompanied by an ~50% decrease of the maximal amplitude of CMF (Table I) and reduction in the half-width of the amplitude distribution histogram of CMF (Fig. 3 *a*) from a value of 10.3 ± 0.32% (n = 27) to 7.6 ± 0.2% (n = 31).

The effect of ATP depletion of RBCs on the dynamic behavior of CMF has been characterized by the power spectra analysis of CMF. The power spectra of CMF of control and ATP-depleted RBCs are shown in Fig. 4 *a*. The power spectrum of ATP-repleted RBCs was not statistically different from that of control RBCs (Fig. 4 *a*). However, both spectra show a clear difference from the power spectra of ATP-depleted RBCs in the frequency range of 0.3–0.7 Hz.

Effect of MgATP on Membrane Fluctuations of RBC Ghosts

The direct effect of MgATP on fluctuations of the membrane–skeleton complex was examined in studies where RBC ghosts, prepared by saponin treatment, were perfused with different concentrations of MgATP. The dependence of CMF of RBC ghosts on MgATP is shown in Fig. 5.

Perfusing RBC ghosts, prepared by saponin treatment of RBCs, with a KCl solution devoid of MgATP, reveals a basal CMF level that is half that in intact RBCs. To eliminate the possibility that these fluctuations may be attributed to a residual ATP that is weakly associated with the membrane–skeleton, the RBC ghosts were preincubated with hexokinase, an ATP trap. No change in the level of CMF was observed after the incubation of the RBC ghosts with 1 mM hexokinase for ≤60 min. Perfusion of RBC ghosts with increasing concentration of MgATP, increased CMF in a dose-dependent manner (Fig. 5). This build-up of membrane fluctuations increased in the range of 0.1–0.5

Table I. The Effect of ATP Depletion on Maximal Amplitude of CMF in RBC

RBC treatment	(ΔI/I)
	%
Control RBC	16.5 ± 3 (n = 122)
RBC without glucose (after 24 h at 37°C)*	9.7 ± 0.7 (n = 26)
RBC with glucose (after 24 h at 37°C)	15.8 ± 1.3 (n = 18)
RBC without glucose (after 16 h at 4°C)*	10.4 ± 2 (n = 91)
RBC with glucose (after 16 h at 4°C)	14.9 ± 2 (n = 59)
RBC with glucose (32 h at 4°C)	14.1 ± 2.7 (n = 17)
RBC with glucose (32 h at 4°C), after 16 h at 4°C without glucose*	14.7 ± 2.3 (n = 27)
RBC without glucose + iodoacetamide (IAA) (after 5 h at 37°C)‡	9.9 ± 1.4 (n = 59)
RBC without glucose + IAA + inosine‡ (after 1 h at 37°C)	10.1 ± 1 (n = 134)
RBC without glucose + IAA + inosine‡ (after 5 h in 37°C)	8.8 ± 1.2 (n = 17)

(ΔI/I)% values are expressed as mean ± SD for n examined cells.
*Reversible ATP depletion.
‡Irreversible ATP depletion.

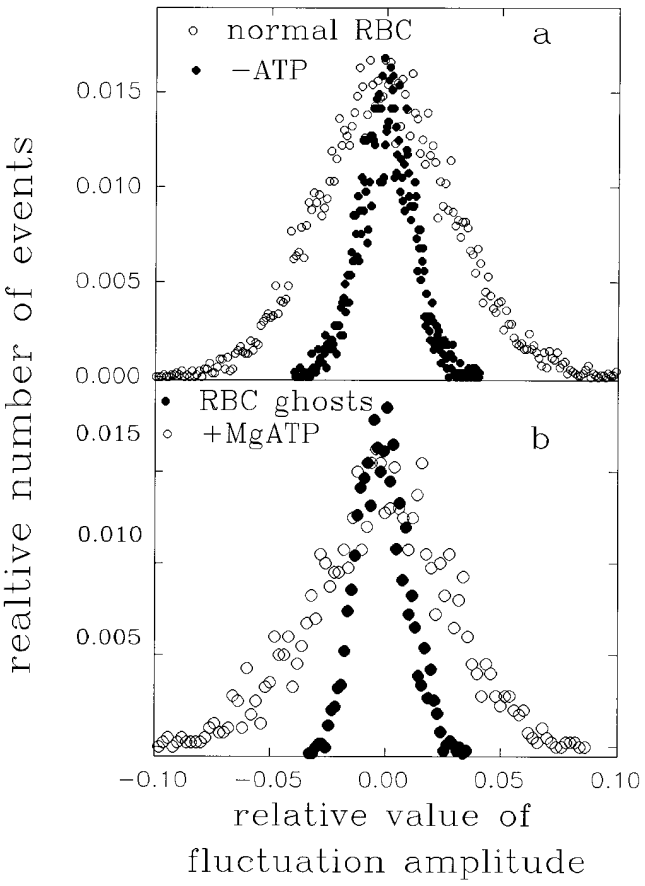

Figure 3. The effect of MgATP on the amplitude histogram of CMF in human RBCs and RBC ghosts. (*a*) Amplitude histogram of CMF in control intact RBCs (*open circle*) and in ATP-depleted RBCs (*closed circle*). (*b*) Amplitude histogram of CMF in RBC ghosts perfused with KCl solution in the absence (*closed circles*) and the presence of 1 mM MgATP (*open circles*). The amplitude histograms were obtained from recordings of time series of light intensity scattering in the range of 0.3–30 Hz. The scattering from each surface area was recorded for 55 or 110 s (sampling rate of 75 points/s). The data analysis procedure, to obtain an amplitude histogram, starts by dividing the whole recorded trace into a number of segments of equal size, where the number of data points within each segment was normalized to the total number of events. Derived probabilities were tabulated and a graph of probabilities was plotted versus values of the grouped data points forming a frequency polygon (an amplitude distribution).

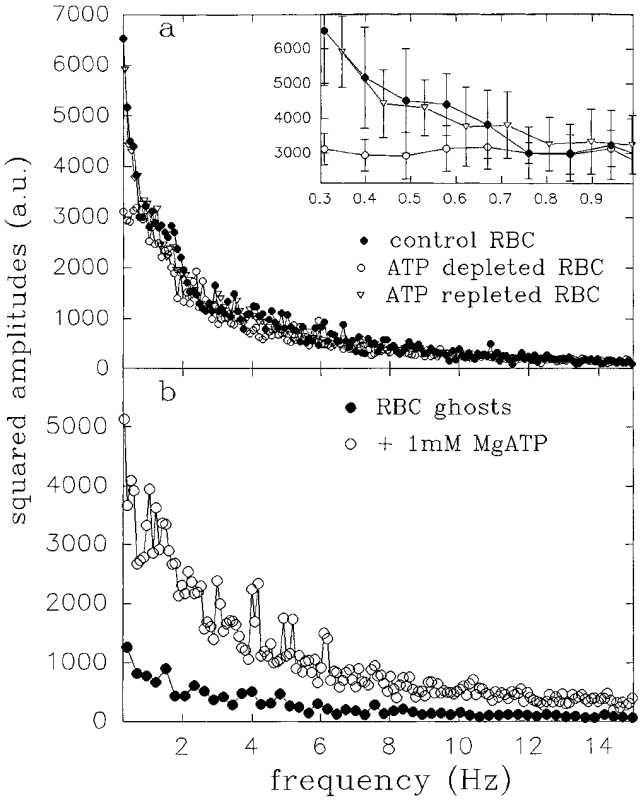

Figure 4. Power spectra of CMF of normal RBCs, ATP-depleted RBCs, and RBC ghosts in the absence and presence of MgATP. (*a*) The power spectra of CMF of normal RBCs (*closed circle*), ATP depleted RBCs (*open circle*) and ATP-repleted RBCs (*open triangles*), each is an average of 15 spectra. The inset of *a* shows an expanded power spectra in the frequency range of 0.3–1 Hz, where the bars are the SD for each data point. (*b*) The power spectra of CMF of RBC ghosts in the presence (*open circle*) and absence (*closed circle*) of 1 mM MgATP, each is an average of six spectra.

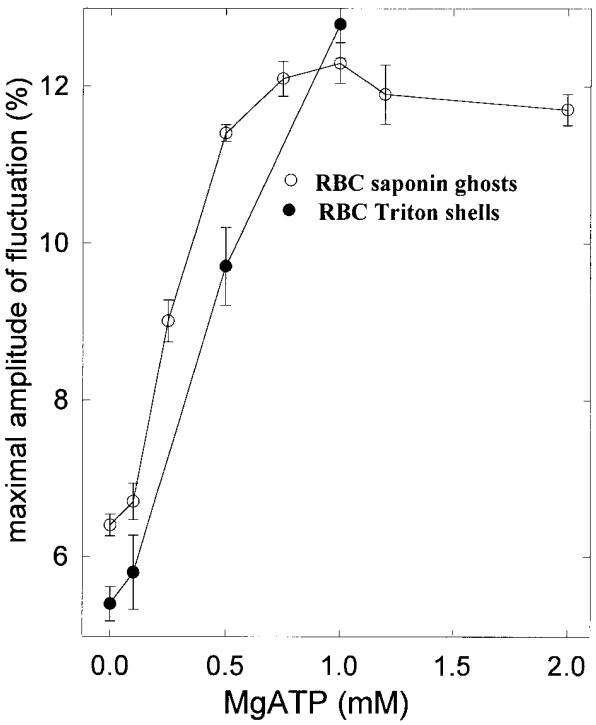

Figure 5. The effect of MgATP concentration on CMF in RBC ghosts (*open circle*) and in Triton X-100–prepared RBC shells (*closed circle*).

mM MgATP and leveled off at the physiological concentration range of 1–2 mM MgATP, reaching the maximal amplitude level exhibited by intact RBCs. The half-width of amplitude distribution histogram of CMF increased from 4.1 ± 0.3% (n = 19), in the absence of MgATP, to 9.1 ± 0.8% (n = 21) in the presence of 1 mM MgATP (Fig. 3 *b*). The effect of MgATP on CMF was reversible, since perfusion of RBC ghost with a KCl solution, after being exposed to MgATP, brought about a decrease of CMF back to its basal level. However, the exposure of the RBC ghosts to a high, non-physiological, concentration of 10 mM MgATP resulted in an irreversible 80% decrease of the maximal amplitude of CMF (data not shown).

The power spectra of CMF in RBC ghosts, in the absence and presence of 1 mM MgATP are given in Fig. 4 *b*. Statistically significant changes between the two spectra are observed in the frequency range of 0.3–5 Hz.

Effect of ATP Analogues on Membrane Fluctuations in RBC Ghosts

To study the mechanism by which MgATP affects CMF, we compared the effect of MgATP to that of non-hydrolyzable ATP analogues. This enables us to differentiate between the MgATP binding and the hydrolysis–phosphorylation steps. The basal level of CMF in RBC ghosts was 6.6 ± 0.7% (n = 18). Perfusion with MgAMP-PNP had no effect on this level yielding 7.3 ± 3.2% (n = 32) and 6.7 ± 2.5% (n = 13) in the presence of 1 mM and 2 mM MgAMP-PNP, respectively. Similarly, MgATPγS had no effect on CMF level yielding 5.8 ± 1.2% (n = 28) in the presence of 0.5 mM MgATPγS.

Whereas MgAMP-PNP alone had no effect on CMF levels, it caused an attenuation of MgATP-stimulated fluctuation as a function of MgAMP-PNP (Fig. 6). Concentrations of 3–4 mM of AMP-PNP were shown to completely abolish the stimulatory effect of 0.5 mM MgATP (Fig. 6). At lower MgATP concentration (0.25 mM) the stimulatory effect was already abolished by 2 mM AMP-PNP. MgATPγS similarly inhibited CMF, but it did so at smaller concentrations. Thus, the CMF level of 10.4 ± 0.7% (n = 19), in the presence of 0.5 mM MgATP, was attenuated to a level of 8.6 ± 1.3% (n = 18) and 6.2 ± 1.2% (n = 29) upon addition of 0.25 mM and 0.5 mM of MgATPγS, respectively.

ATP analogues, MgGTP, and MgITP, were ineffective for elevating CMF levels. CMF levels of 6.7 ± 2.0% (n = 58) and 6.3 ± 1.7% (n = 37) were measured in the presence of 1 mM and 2 mM of MgGTP, respectively. Incubation with 1 mM and 2 mM MgITP yielded CMF levels of 5.7 ± 1.3% (n = 26) and 6.3 ± 1.7% (n = 37), respectively.

Effect of MgATP on Skeleton Fluctuations in Triton X-100 Shells of RBCs

The stimulatory effect of MgATP on CMF levels in RBC

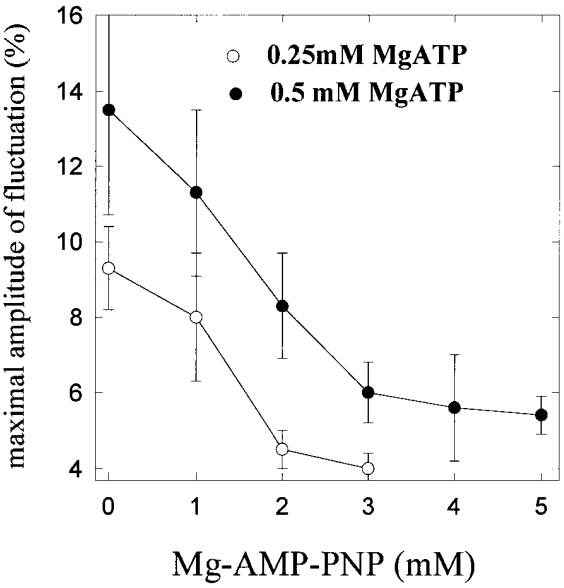

Figure 6. The effect of MgAMP-PNP concentration on CMF in RBC ghosts in the presence of 0.25 mM MgATP (*open circle*) and 0.5 mM MgATP (*closed circle*).

ghosts can be mediated either through its direct effect on plasma membrane components or by affecting the underlying protein network of the RBC's skeleton. To discriminate between these two possibilities we examined CMF in Triton X-100 shells of RBCs, which are composed of the skeleton network, devoid of the plasma membrane. Perfusion of Triton X-100 shells with a buffered KCl solution resulted in a low basal level of fluctuation, which is less than half its value in intact RBCs (Figs. 5 and 7). Perfusion with increasing concentrations of MgATP restored the fluctuation amplitude to a level similar to that measured in intact RBCs (Figs. 5 and 7). However, this restoration of fluctuation was only a transient one and vanished together with an irreversible shrinkage of the skeleton shell 30 min after solubilization by Triton X-100 of the bilayer in the RBC ghost. Within this time window, the skeleton's fluctuations increased, in the presence of 0.1–1 mM MgATP, to the same CMF levels observed either in RBC ghosts, in the presence of 1 mM MgATP, or in intact RBCs. Again, the stimulatory effect of MgATP on CMF was reversible. Perfusion of skeleton shells with a KCl solution, after exposure to MgATP, caused the decline of CMF to the basal level.

Short heat treatment of the intact RBC, under conditions known to induce dissociation and denaturation of the skeleton from the membrane (Vertessy and Steck, 1989) led to a drop of CMF from a level of 14.8 ± 6.4% (n = 10) down to 5 ± 4.9% (n = 37) ($P < 0.01$). The heat treatment was not accompanied by any significant shape change of RBCs.

Effect of Vanadate on MgATP-induced CMFs and on Phosphorylation of the Membrane–Skeleton

Vanadate is a known inhibitor of ATPases and phosphatases in cells, presumably because it adopts a stable structure that resembles the transition state of phosphate (Beauge and Glynn, 1978). The CMF level of 14.6 ± 1.3% (n = 32) in intact RBCs decreased to a level of 10.6 ± 1% (n = 22) after 15 min preincubation with 30 μM vanadate. Preincubation in the presence of higher vanadate concentrations of 0.1 mM and 1 mM did not result in additional decrease of CMF, yielding levels of 11.3 ± 1.2% (n = 14) and 11.2 ± 2 % (n = 9), respectively.

Vanadate also exerted its inhibitory effect on MgATP-induced CMF in RBC ghosts. Perfusion of RBC ghosts with 1 mM MgATP resulted in a high CMF level of 11.7 ± 1.4% (n = 22). However, in the presence of 10 μM vanadate the stimulatory effect of MgATP was completely lost, leading to a low CMF level of 5.7 ± 1.2% (n = 21). Further increase of vanadate concentration to 0.1 mM and 1 mM did not result in any further changes of CMF, as reflected by CMF levels of 5.9 ± 1.3% (n = 25) and 6.1 ± 1.6% (n = 12), respectively. It should be noticed that whereas in the intact RBC the vanadate caused a ~30% decline, the CMF level in RBC ghosts exposed to 1 mM MgATP decreased by 50% in the presence of vanadate.

Immunoblot analysis of the basal level of phosphotyrosine in the membrane–skeleton of intact RBCs failed to detect phosphorylated tyrosine. However, 15 min preincubation of RBCs with 30 μM vanadate, resulted in the formation of a moderate level of phosphotyrosine associated with band 3. Similar exposure of RBC ghosts to 1 mM

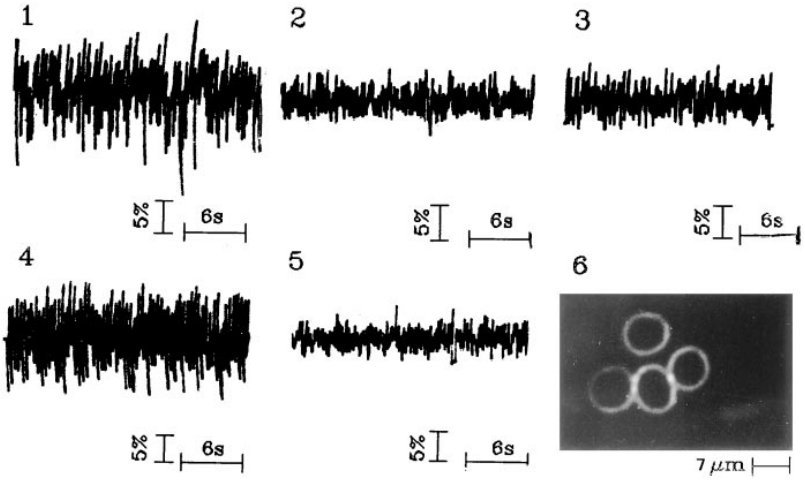

Figure 7. Recordings of time-dependent light scattering from the side surface of Triton X-100 shells in the absence and presence of 1 mM MgATP. Intact RBCs (0.1% hematocrit) were first converted into RBC ghosts by perfusing intact RBCs with 0.0075% saponin. Triton X-100 shells were prepared by treating the RBC ghosts with 0.04% Triton X-100. The recording of CMF are shown for the following states: (*1*) Intact RBC; (*2*) RBC ghost; (*3*) Triton X-100 shell; (*4*) Triton X-100 shell in the presence of 1 mM MgATP; (*5*) Triton X-100 shell after contraction; (*6*) Dark field microscopic images of Triton X-100 shells (before contraction). Bar, 7 μm.

MgATP, in the presence of 10 μM vanadate resulted in very strong phosphorylation of tyrosine on band 3. However, no phosphorylation was obtained in the absence of vanadate. Similar analysis of phosphoserine in intact RBCs and RBC ghosts showed a significant basal level of phosphorylation although no change in the phosphorylation level was observed in the presence of vanadate.

Effect of Phalloidin, DNase I, and Cytochalasins on MgATP-induced CMFs

Phalloidin, is known to specifically and tightly bind to F-actin (De La Cruz and Pollard, 1994). Since phalloidin was also found to inhibit actin's ATPase in the membrane–skeleton of human erythrocytes (Sato et al., 1986), we examined its effects on CMF. The basal level of CMF in RBC ghosts was 6.3 ± 1.3% (n = 16). Preincubation of RBC ghosts with 5 μM phalloidin did not affect the level of CMF (6.2 ± 1.8%; n = 25). However, perfusion of 1 mM MgATP-treated RBC ghosts with phalloidin, was found to inhibit the MgATP-dependent CMF in a concentration-dependent manner (Fig. 8). The elevation of CMF to 13.5 ± 2.2% (n = 55) in RBC ghosts by 1 mM MgATP was unaffected by preincubation with phalloidin in the concentration range of 0.44–1 μM. However, at phalloidin concentrations of 1.5–4 μM, CMF amplitudes were gradually diminished, down to the basal level of 6.2 ± 0.8% (n = 29) (Fig. 8). Similar experiments with DNase I, in the presence of 1 mM MgATP, show that the CMF level of 16 ± 1% (n = 21), drop to a level of 6 ± 0.8% (n = 35) after 15 min preincubation with 0.16 μM DNase I. The half-width of amplitude distribution in CMF of ghosts, in the presence of 4.4 μM phalloidin or 0.16 μM DNase I decreased from 9% to 6%, and 3%, respectively (Fig. 9). The three-dimensional sectioning of RBC ghost population, labeled with phalloidin-rhodamine (Fig. 10 *A*) or DNase I–FITC in the presence of phalloidin-rhodamine (Fig. 10 *B*), shows similar dimensions to those of intact RBCs (~8-μm diam and ~1.5-μm thick). The labeling of F-actin by phalloidin-rhodamine seems to be spread all over the membrane–skeleton, revealing phalloidin-rhodamine patches rather than uniform distribution. This pattern was observed both in fixed and non-fixed RBC ghosts. The binding of phalloidin-rhodamine and DNase I–FITC to the same RBC ghosts is shown in Fig. 10 *B*. This figure shows that the prelabeling of the RBC's F-actin with phalloidin-rhodamine (4.4 μM) did not inhibit the binding of DNase I–FITC (35 nM) to the F-actin. Again, non-homogeneous distribution appears to be a property possessed not only by phalloidin-rhodamine but also by DNase I–FITC (Fig. 10 *B*, *inset*). Moreover, we observe (Fig. 10 *B*, *inset*) the occurrence of three labeled subpopulations: sites that bind solely phalloidin-rhodamine (red) or DNase I–FITC (green), as well as sites that bind both (yellow).

The level of CMF of 15 ± 2.1% (n = 18) in intact RBCs was not affected by exposure of RBCs to 2 μM dihydrocytochalasin B for 24 h at room temperature (14.2 ± 1.9%; n = 23) or to 4 μM dihydrocytochalasin B for 30 min (14.4 ± 1.6%; n = 7). However, exposure of RBCs to 20 μM cytochalasin D for 2 h resulted in a minor statistically significant (P = 0.004) increase in CMF from 14.9 ± 2.9% (n = 119) to 16.9 ± 3.9% (mean ± SEM) (n = 119).

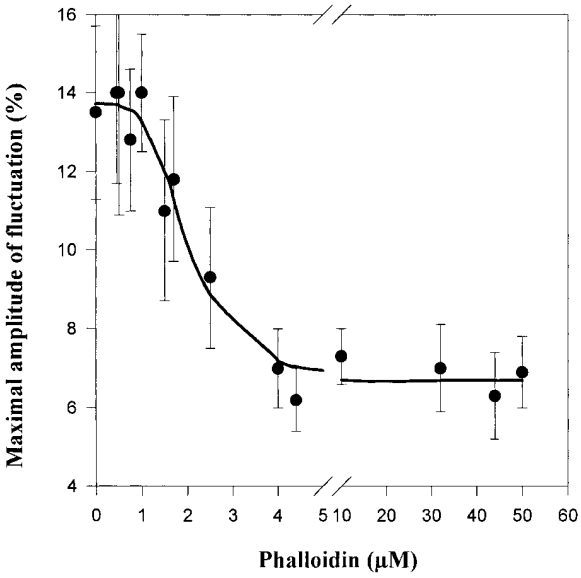

Figure 8. The effect of phalloidin on the maximal amplitude of CMF in RBC ghosts in the presence of 1 mM MgATP.

Discussion

ATP depletion in intact RBCs, after prolonged incubation (24 h) without the glycolysis physiological substrate, leads to reduction in the amplitude characteristics of CMF. Thus, we observe a 26% decrease of the half-width of amplitude distribution and a 40% decrease of the maximal CMF level in ATP-depleted discoid RBCs, as compared with RBCs stored under identical conditions but in the presence of glucose. This decrease of the maximal CMF level is two- to fourfold larger than the variation coefficient of CMF in control RBCs. It should be pointed out that there exists a three- to fivefold time-delay between the process of ATP depletion and the actual shape change of RBCs (Ferrell and Huestis, 1984; Backman, 1986). In this case, RBC crenated after 5–7 h following 95% of ATP depletion (Ferrel and Huestis, 1984). To avoid "aging" processes, resulting from the long incubation time needed to decrease intracellular ATP, we used fast procedures for ATP depletion based on the use of glycolysis inhibitors. The shorter and more drastic depletion procedure, based on the incubation of RBCs in the presence of iodoacetamide and inosine, resulted in a 50% drop in the maximal fluctuation amplitude. Therefore, it may be suggested that the excessive attenuation of CMF in ATP-depleted RBCs is independent of the depletion procedure.

To resolve whether the MgATP binding sites are associated with a cytosolic component(s) or with the membrane–skeleton, we investigated the MgATP effects in RBC ghosts. The observation that perfusion of open RBC ghosts with MgATP alone leads to reversible reconstitution of membrane–skeleton mechanical fluctuations to their level in the intact RBC implies that MgATP exerts its effect directly on the membrane–skeleton complex rather than transducing it via a cytosolic component. The relative contributions of the plasma membrane and the underlying skeleton to CMF emerges from studying CMF in skeleton shells. Incubation of skeleton shells with MgATP resulted

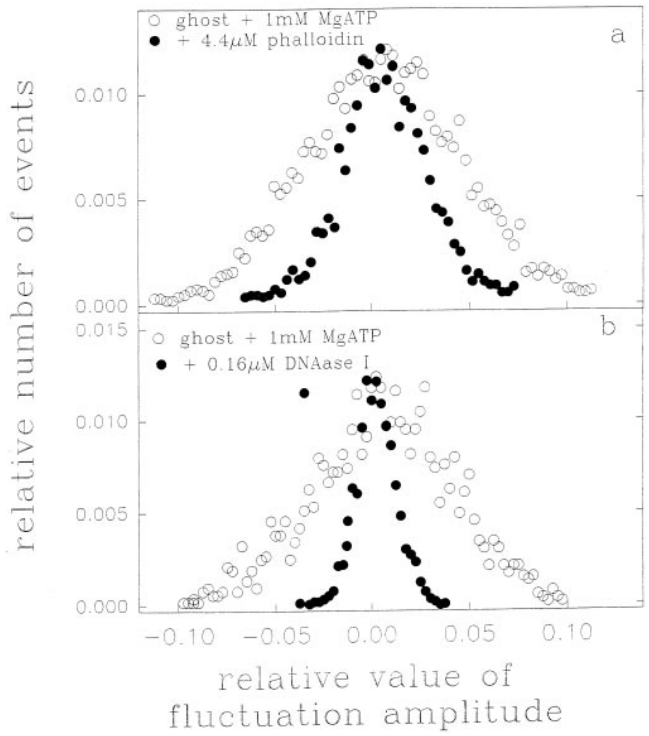

Figure 9. The effect of phalloidin or DNase I on amplitude distribution of CMF in RBC ghosts, which were perfused with MgATP. (*a*) Amplitude distribution of CMF in RBC ghosts after perfusion with MgATP (*open circle*) and 1 mM MgATP + 4.4 μM phalloidin (*closed circle*). (*b*) Amplitude distribution of CMF in RBC ghosts after perfusion with MgATP (*open circle*) and 1 mM MgATP + 0.16 μM DNAse I (*closed circle*).

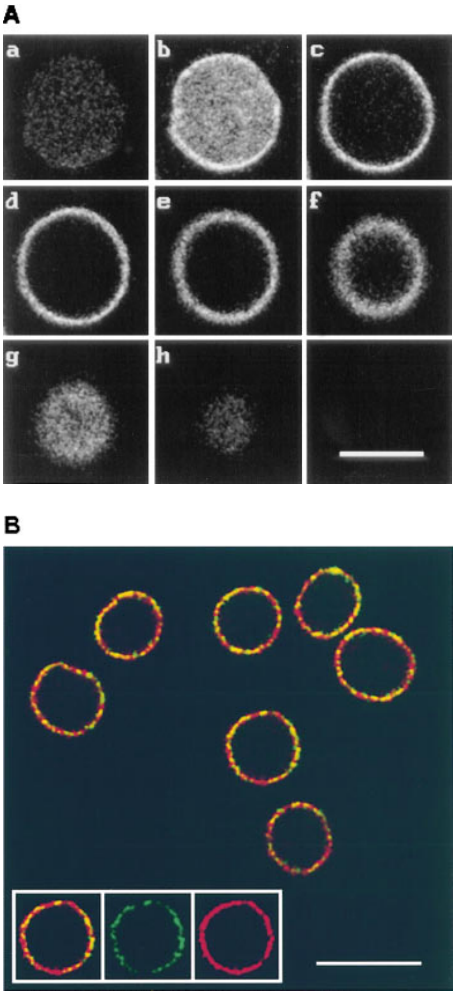

Figure 10. The spatial distribution of actin in RBC ghosts revealed by fluorescent probes of phalloidin-rhodamine and DNase I–FITC. The spatial distribution of the fluorescent probes was analyzed via a three-dimensional optical sectioning by a confocal inverted laser scanning microscope. (*A*) Optical sections (*a–h*, 0.6 μm apart) of RBC ghost labeled by phalloidin-rhodamine (4.4 μM). Each square of the gallery of images possesses a dimension of 9.5 μm × 9.5 μm. (*B*) The distribution of phalloidin-rhodamine and DNase I–FITC in RBC ghosts in an optical section taken at the middle (half thickness) of the RBC ghost. *Inset*, The separate distribution of phalloidin-rhodamine (*red*) and DNase I (*green*) in a RBC ghost that was labeled with both phalloidin-rhodamine and DNase I–FITC. Bars: (*A*) 5 μm; (*B*) 10 μm.

in the elevation of CMF, as a function of MgATP concentration, up to their levels in intact RBCs. These findings show that MgATP-dependent mechanical displacements of the skeleton are responsible for CMF. This is further supported by our observation that exposing RBCs and RBC ghosts to conditions known to cause dissociation and denaturation of the membrane-skeleton, either by short heat treatment of RBCs (Vertessy and Steck, 1989) or by incubating RBC ghosts with high concentrations (8–25 mM) of ATP (Sheetz and Casaly, 1980) leading to drastic irreversible attenuation in CMF levels (data not shown). It should be pointed out that MgATP-dependent CMF of skeleton shells are maintained in the absence of 95% of the bilayer's phospholipids extracted by Triton X-100 (Sheetz, 1979). This suggests that MgATP-stimulated fluctuations are independent of the lipid bilayer.

The specificity of the MgATP effect was tested by using other nucleotides such as MgGTP or MgITP. These two nucleotides, within the concentration range examined, had no effect on CMF, suggesting that the stimulation sites are specific for MgATP. The ability to differentiate between the effect of MgATP binding and the possible consequent hydrolysis-phosphorylation processes was examined by using non-hydrolyzable ATP analogues. The fact that CMF are not affected by non-hydrolyzable analogues of ATP, such as AMP-PNP and ATPγS (which actually possesses an extremely low rate of hydrolysis), implies that the cleavage of the γ-phosphate bond is necessary for the stimulatory effect to occur. This is supported by the observed inhibition of the stimulatory effect of MgATP in the presence of MgAMP-PNP or MgATPγS, resulting from competition for the binding sites on the membrane–skeleton. The higher inhibitory effect of ATPγS, as compared with that of AMP-PNP, may be attributed to the higher affinity of ATPγS to the nucleotide-binding site, similarly to the data obtained for the ATPase of the molecular chaperone Dnak (Theyssen et al., 1996).

MgATP may exert its stimulatory effect on CMF via membrane–skeleton-associated ATPase and/or changing the phosphorylation state of the membrane–skeleton by the kinase-phosphatase system. An initial attempt to resolve this question was carried out by analyzing the effect

of vanadate, an inhibitor of ATPases and phosphotyrosine phosphatase, on CMF and on membrane–skeleton phosphorylation. A major inhibition of CMF was observed after a 15-min preincubation of intact RBCs or RBC ghosts with 30 μM and 10 μM vanadate, respectively. Analysis of phosphorylation of the membrane–skeleton, under similar conditions, did not reveal any significant change in serine phosphorylation associated with spectrin. This finding confirms a previous study that similarly showed, using ^{32}P incorporation, no change in spectrin phosphorylation in the presence of vanadate (Patel and Fairbanks, 1986). However, under similar incubation of RBCs or RBC ghosts with vanadate minor and major phosphorylation of band 3 tyrosine, respectively, were observed. It has been shown that spectrin phosphorylation by casein kinase I affects the mechanical stability of the RBC (Manno et al., 1995). Thus, it may be speculated that tyrosine phosphorylation in the cytoplasmic domain of band 3 may increase the rigidity of the membrane–skeleton, leading to the attenuation of CMF. Nevertheless, it is possible that phosphorylation leads to a minor inhibitory effect of vanadate on CMF, whereas the major effect is elicited via the inhibition of skeleton's ATPase. Indeed, the ability to associate the MgATP stimulatory binding sites with ATPase activity sites is in agreement with a previous finding that showed that 10 μM vanadate caused a 35% inhibition of ATPase activity in normal and salt-extracted RBC ghosts (Patel and Fairbanks, 1986).

If one assumes direct proportionality between MgATP binding to its stimulatory sites and the increase in fluctuation amplitude, it is possible to estimate the order of the equilibrium constant for this activation process. By doing so, we obtain an apparent dissociation constant, K_d (calculated from the EC_{50}) of 0.29 mM. This value is close to the K_d of 0.4 mM obtained for the low affinity Mg^{+2}-dependent ATPase activity in RBC ghosts (Morris et al., 1993). ATPase activity was shown to be associated with the skeleton and particularly with the spectrin–actin–protein 4.1 complex (Sato et al., 1986; Morris et al., 1993). Both spectrin and protein 4.1 were found to be devoid of ATPase activity, leaving actin as the main candidate to possess ATPase activity (Sato et al., 1986). The identification of the skeleton's ATPase activity with that of actin's ATPase was confirmed by experiments where 95% of this Mg^{+2}-dependent ATPase activity was inhibited by specific actin ligands: phalloidin and DNase I (Sato et al., 1986).

The involvement of actin's ATPase in MgATP stimulation of CMF in RBC ghosts or skeleton shells is suggested by the inhibition of MgATP-dependent CMF by phalloidin and DNase I. Phalloidin was found to abolish CMF at concentrations higher than 4 μM (EC_{50} of ~2 μM), which were previously shown to completely inhibit the MgATPase activity of the RBC's skeleton (Sato et al., 1986). Based on the known binding constant of phalloidin to skeletal muscle F-actin (K_d ~2–7 nM; Huang et al., 1992; Allen et al., 1996; De La Cruz and Pollard, 1996) we can estimate that at 2 μM phalloidin, 99.6% of the binding sites of F-actin are occupied by phalloidin. This suggests that both Mg-dependent ATPase activity and CMF are abolished only when complete occupancy of phalloidin binding sites on F-actin is achieved. If F-actin in erythrocytes undergoes an effective depolymerization–polymerization process, phalloidin should shift the equilibrium towards F-actin. This by itself may lead to change in the mechanical properties of actin (Janmey et al., 1994). However, the fact that phalloidin (5 μM) was unable to alter the basal level of CMF in RBC ghosts, in the absence of MgATP, may suggest that the binding of phalloidin to the surface of F-actin does not alter the mechanical properties of the membrane–skeleton in the RBC. This is supported by the observation that phalloidin binding to actin did not increase the ratio of storage/loss shear moduli of β-actin (Allen et al., 1996).

The specific binding of dihydrocytochalasin B or the more potent cytochalasin D to the barbed end (fast growing, positive) of F-actin had either no, or a small effect on CMF, respectively. This may suggest that the minor effect of cytochalasins can be attributed to the very low polymerization–depolymerization of RBC's F-actin (Pinder and Gratzer, 1983, Pinder et al., 1986), and the accompanying ATP hydrolysis and nucleotide exchange near the barbed end (Korn et al., 1987). Moreover, cytochalasins showed no effect on Mg-ATPase activity, even at high concentrations (Sato et al., 1986). However, the unique association of DNase I with the pointed end of F-actin (Podolski and Steck, 1988) was found to abolish CMF of RBC ghosts at a concentration of 0.16 μM, which was effective in bringing about a complete inhibition of the skeleton's MgATPase (Sato et al., 1986). Under these conditions, the theoretical occupancy of the pointed end of erythrocyte's F-actin by DNase I should be 99% (assuming a K_d of ~2 nM; Podolski and Steck, 1988). These findings are in agreement with the recent observation of CMF attenuation by DNase I (Krol, A.J., M.G. Grinfeldt, and V.V. Malev. 1995. *Biophys. J.* 74:A286, abstract from *Annu. Gen. Meeting Am. Biophys. Soc., 39th, San Francisco, CA, W-Pos172*). Comparison of the fully inhibitory effects of phalloidin and DNase I on CMF of RBC ghosts demonstrates that DNase I reduces the half-width of the amplitude distribution 1.5-fold more than the decrease caused by phalloidin (Fig. 9). This may reflect that the more effective inhibition of CMF occurring via binding of DNase I to the pointed end of F-actin.

The fact that most of the ATPase activity in the membrane–skeleton of RBCs is associated with F-actin and is inhibited by DNase I (Sato et al., 1986), together with the finding that DNase I binds to the pointed end of F-actin (Podolski and Steck, 1988), suggests that most of F-actin's ATPase activity is located at its pointed end. Therefore, we would like to suggest that the actin's ATPase, located at the pointed end of the short (33 ± 5 nm) actin filament, is responsible for the MgATP stimulation of CMF in intact RBCs, RBC ghosts, and skeleton shells. This suggestion is in agreement with previous proposals that an actin-based contractile system may be involved in the shape change of erythrocytes (Weed et al., 1969; Schrier et al., 1981). The possible existence of such a contractile system in human erythrocytes is supported by studies that show the existence of membrane bound myosin II in human erythrocytes (Der Terrossian et al., 1994; Fowler et al., 1985; Wong et al., 1985). This is compatible with the observation that protein 4.1 binds and modulates actin-activated MgATPase activity of myosin, when using isolated protein assays (Pasternack and Racusen, 1989).

The non-homogenous labeling of actin, as revealed by confocal microscopy (Fig. 10), is in agreement with the

previously shown punctate pattern of actin obtained by immunofluorescent based non-confocal microscopy (Der Terrossian et al., 1994). It may be speculated that the non-uniform labeling of actin is due to the non-homogenous distribution of actin in the membrane-skeleton. Previous studies suggest that the pointed end of F-actin in erythrocytes is capped by spectrin-4.1 complex (Pinder et al., 1984) and/or by tropomodulin (Ursitti and Fowler, 1994; Fowler, 1996). Thus, an additional cause to the non-uniform pattern may originate from the partial capping of F-actin, where the capped actin is protected from labeling.

The dynamic characteristics of the MgATP-dependent mechanical fluctuations are revealed by the power spectrum of CMF. The analysis of the power spectra of CMF in either normal RBCs or ATP-depleted ones shows no statistically significant spike, suggesting that CMF, under either condition, are non-periodic. The power spectrum can serve to estimate the energy released in the studied CMF, whereas the energy content of the process can be estimated from the amplitude histogram of CMF. The amplitude histograms given in Fig. 3 clearly demonstrate that the fluctuation energy of the erythrocyte's membrane–skeleton complex in ATP-depleted cells is smaller than in normal RBCs. Similarly, the fluctuation energy of RBC ghosts is larger in the presence of MgATP than in its absence. Moreover, the energy content in the presence of phalloidin and DNase I is similar to the one obtained in the absence of MgATP. These conclusions coincide with the qualitative information obtained from the power spectrum changes. The energy difference, both in intact RBCs and in RBC ghosts, is confined to the low frequency region of the power spectra (0.3–5 Hz). These two significant features are in accord with our hypothesis about the existence of a metabolic driving force in addition to the thermal one (Tuvia et al., 1997). This metabolic component can be associated with a specific enzymatic reaction involving the actin–ATPase activity, which serves as an energy source for mechanical fluctuations of the membrane–skeleton. Thus, the known turnover of the actin's ATPases in the RBC of 0.01–0.02 mol Pi/mol F-actin $\times$ s (Morris et al., 1993) may correspond to a periodic fluctuation at the low frequency range. However, if one takes into account that the illuminated area ($\sim$0.25 μm^2) contains a hundred actin containing junctions with the ATPase reaction occurring at each junction independently of all others, i.e., that reactions at the different sites are not synchronized, than the overall energy input will be random, producing the aperiodic characteristics of CMF.

We would like to acknowledge the help of A. Krol, Y. Zipser, A. Barbul, L. Mittelman, and A. Pinchasov.

This research was supported by grants from the Office of Naval Research (3N00014-94-1-5 to S. Levin and R. Korenstein) and the US-Israel Binational Science Foundation (No. 91-00209 to R. Korenstein and S. Levin). This research is part of a doctoral thesis by S. Tuvia.

Received for publication 19 February 1998 and in revised form 30 April 1998.

References

Allen, P.G., C.B. Shuster, J. Käs, C. Chaponnier, P.A. Janmey, and I.M. Herman. 1996. Phalloidin binding and rheological differences among actin isoforms. *Biochemistry.* 35:14062–14069.

Backman, L. 1986. Shape control in human red blood cell. *J. Cell Sci.* 80:281–298.

Beauge, L.A., and I.M. Glynn. 1978. Vanadate inhibits the red cell sodium potassium ATPase from the cytoplasmatic side. *Nature.* 272:552–554.

De La Cruz, E.M., and T.D. Pollard. 1994. Transient kinetic analysis of rhodamine phalloidin binding to actin filaments. *Biochemistry.* 33:14387–14392.

De La Cruz, E.M., and T.D. Pollard. 1996. Kinetics and thermodynamics of phalloidin binding to actin filaments from three divergent species. *Biochemistry.* 35:14054–14061.

Der Terrossian, E., C. Deprette, I. Lebbar, and R. Cassoly. 1994. Purification and characterization of erythrocyte caldesmone. *Eur. J. Biochem.* 219:503–511.

Ferrell, J., and W.H. Huestis. 1984. Phosphoinosite metabolism and the morphology of human erythrocytes. *J. Cell Biol.* 98:1992–1998.

Fowler, V.M. 1996. Regulation of actin filament length in erythrocytes and striated muscle. *Curr. Opin. Cell Biol.* 8:86–96.

Fowler, V.M., J.Q. Davis, and V. Bennett. 1985. Human erythrocyte myosin: Identification and purification. *J. Cell Biol.* 100:47–55.

Glynn, I.M., and V.L. Lew. 1970. Synthesis of adenosine triphosphate at the expense of downhill cation movement in intact human red blood cells. *J. Physiol. (Lond.).* 207:393–399.

Huang, Z.J., R.P. Haugland, W.M. You, and R.P. Haugland. 1992. Phallotoxin and actin binding assay by fluorescence enhancement. *Anal. Biochem.* 200: 199–204.

Janmey, P.A., S. Hvidt, J. Kist, D. Lerche, A. Maggs, E. Sackmann, M. Schliwa, and T.P. Stossel. 1994. The mechanical properties of actin gels. *J. Biol. Chem.* 51:32503–32513.

Korn, E.D., M.F. Carlier, and D. Pantaloni. 1987. Actin polymerization and ATP hydrolysis. *Science.* 238:638–644.

Krol, A.J., M.G. Grinfeldt, S.V. Levin, and A.D. Smilgavichus. 1990. Local mechanical oscillations of the cell surface within range 0.2-30 Hz. *Eur. Biophys. J.* 19:93–99.

Levin, S.V., and R. Korenstein. 1991. Membrane fluctuations in erythrocytes are linked to MgATP-dependent dynamic assembly of the membrane skeleton. *Biophys. J.* 60:733–737.

Lew, V.L., and H.G. Ferreira. 1978. Calcium transport and the properties of a calcium-activated potassium channel in red cell membranes. *Curr. Top. Membr. Transp.* 10:217–277.

Lew, V.L., and J. Gracia-Sancho. 1989. Measurement and control of intracellular calcium in intact red cells. *Methods Enzymol.* 173:100–112.

Manno, S., Y. Takakuwa, K. Nagao, and N. Mohandas. 1995. Modulation of erythrocyte membrane mechanical function by betaspectrin phosphorylation and dephosphorylation. *J. Biol. Chem.* 270:5659–5665.

Mittelman, L., S. Levin, and R. Korenstein. 1991. Fast cell membrane displacements in B lymphocytes: Modulation by dihydrocytochalasin B and colchicine. *FEBS (Fed. Eur. Biochem. Soc.) Lett.* 293:207–210.

Mittelman, L., S. Levin, H. Verschueren, P. De-Baetselier, and R. Korenstein. 1994. Direct correlation between cell membrane fluctuations, cell filterability and the metastatic potential of lymphoid cell lines. *Biochem. Biophys. Res. Commun.* 203:899–906.

Morris, B.M., M.E. Auland., Y.H. Xu, and B. Roufogails. 1993. Characterization of the MgATPase activity of the human erythrocyte membrane. *Biochem. Mol. Bio. Int.* 21:823–832.

Patel, V.P., and G. Fairbanks. 1986. Relationship of major phosphorylation reactions and MgATPase activities to ATP-dependent shape change of human erythrocyte membranes. *J. Biol. Chem.* 261:3170–3177.

Pasternack, G.R., and R.H. Racusen. 1989. Erythrocyte protein 4.1 binds and regulates myosin. *Proc. Natl. Acad. Sci. USA.* 86:9712–9718.

Peterson, M.A., H. Strey, and E. Sackman. 1991. Theoretical and phase contrast microscopic eigenmode analysis of erythrocyte flicker: amplitudes. *J. Phys. II France* 2:1273–1285.

Pinder, J.C., and W.B. Gratzer. 1983. Structural and dynamic states of actin in the erythrocyte. *J. Cell Biol.* 96:768–775.

Pinder, J.C., V. Ohanian, and W.B. Gratzer. 1984. Spectrin and protein 4.1 as an actin filament capping. *FEBS (Fed. Eur. Biochem. Soc.) Lett.* 169:161–164.

Pinder, J.C., Weeds, A.G., and W.B. Gratzer. 1986. Study of actin filament ends in the human red blood cell membrane. *J. Mol. Biol.* 191:461–468.

Podolski, J.L., and S.L. Steck. 1988. Association of deoxyribonuclease I with the pointed ends of actin filaments in human red blood cell membrane skeletons. *J. Biol. Chem.* 263:638–645.

Rosemberg, Y., and R. Korenstein. 1997. Low electric fields induce endocytotic-like processes: a novel method for incorporation of macromolecules into living cells. *Bioelectrochem. Bioenerg.* 42:275–281.

Sato, S., Y. Jinbu, and M. Nakao. 1986. Characterization of human erythrocyte cytoskeletal ATPase. *J. Biochem.* 100:643–649.

Schrier, S.L., B. Hardy, I. Junga, and L. Ma. 1981. Actin activated ATPase in human red cell membrane. *Blood.* 58:953–962.

Sheetz, M.P. 1979. Integral membrane protein interaction with Triton cytoskeletons of erythrocytes. *Biochim. Biophys. Acta.* 557:122–134.

Sheetz, M.P., and J. Casaly. 1980. 2,3Diphosphoglycerate and ATP dissociate erythrocyte membrane skeletons. *J. Biol. Chem.* 255:9955–9960.

Strey, H., M.A Peterson, and E. Sackman. 1995. Measurements of erythrocyte membrane elasticity by flicker eigenmode decomposition. *Biophys. J.* 69: 478–488.

Theyssen, H., H.P. Schuster, L. Packschies, B. Bukau, and J. Reinstein. 1996. The second step of ATP binding to DnaK induces peptide release. *J. Mol.*

Biol. 263:657–670.

Tuvia, S., S. Levin, and R. Korenstein. 1992*a*. Oxygenation - Deoxygenation cycle of erythrocytes modulates the submicron cell membrane fluctuations. *Biophys. J.* 63:599–602.

Tuvia, S., S. Levin, and R. Korenstein. 1992*b*. Correlation between local cell membrane displacements and filterability of human red blood cells. *FEBS (Fed. Eur. Biochem. Soc.) Lett.* 304:32–36.

Tuvia, S., A. Almagor, A. Bitler, S. Levin, R. Korenstein, and S. Yedgar. 1997. Cell membrane fluctuations are regulated by medium macroviscosity: evidence for a metabolic driving force. *Proc. Natl. Acad. Sci. USA*. 94:5045–5049.

Ursitti, J.A., and V.M. Fowler. 1994. Immunolocalization of tropomodulin, tropomyosin and actin in spread human erythrocyte skeletons. *J. Cell Sci.* 107: 1633–1639.

Vertessy, B.G., and T.L. Steck. 1989. Elasticity of the human red cell membrane skeleton: effects of temperature and denaturants. *Biophys. J.* 55:255–262.

Weed, I., P.L. La Celle, and E.W. Merrill. 1969. Metabolic dependence of red cell deformability. *J. Clin. Invest*. 48:795–809.

Wong, A.J., D.P. Kiehart, and T.D. Pollard. 1985. Myosin from human erythrocytes. *J. Biol. Chem.* 260:46–49.

Zamir, N., S. Tuvia, R. Riven-Kreitman, S. Levin, and R. Korenstein. 1992. Atrial natriuretic peptide: direct effects on human red blood cell dynamics. *Biochem. Biophys. Res. Commun.* 188:1003–1009.

Zipser, Y., and N.S. Kosower. 1996. Phosphotyrosine phosphatase associated with band 3 protein in human erythrocyte membrane. *Biochem. J.* 314:881–887.